New control scheme for four-port grating beam splitter with HfO_2 layer

JINHAI HUANG, BO WANG*, WEIYI YU, JIAHAO LI, XIAOFENG WANG, HONG ZOU, LIQUN LIU, LINJIAN HUANG, XU YANG, GUODING CHEN, QU WANG, LI LUO, LIANG LEI
School of Physics and Optoelectronic Engineering, Guangdong University of Technology, Guangzhou 510006, China

In this paper, a transmission four-port grating beam splitter with 0th order rejection is proposed. Under normal incident conditions, the grating parameters were optimized using rigorous coupled wave analysis and simulated annealing algorithm, and the diffraction efficiency of the optimized grating is 24.24% and 24.34% for the ±1st and ±2nd orders under transverse electric polarization, respectively, and 24.16% and 23.21% for the ±1st and ±2nd orders under transverse magnetic polarization. In addition, the electric field distribution of the grating was analyzed using the finite element method, and the diffraction phenomenon of the grating was analyzed using the simplified modal method. Most importantly, the grating has good polarization-independent spectral performance. The data show that the grating structure has high processing tolerance and is advantageous in the field of beam splitters.

(Received January 21, 2023; accepted August 7, 2023)

Keywords: Four-port, Beam splitter, Transmission grating, Under normal incidence

1. Introduction

The grating [1, 2] is an important part of many optical devices, such as optical (de)multiplexers [3-5] beam splitters [6, 7], lasers elements [8, 9], optical sensors [10-12], etc. Among them, grating beam splitter is an important optical element with high resolution, which can divide the incident light into multiple beams with the same characteristics. It is widely used in fields such as optical communication [13-16], displacement measurement [17], and optical storage [18, 19]. The grating beam splitter with polarization - independent characteristics has stable and parallel multiplexing performance, which can meet the requirements of high efficiency and high laser threshold for high-power lasers. With the development of manufacturing technology, the size of grating is reduced and the efficiency is greatly improved, which makes the grating beam splitter become a research hotspot in the optical, optoelectronic industry. Under this background, people have designed various new types of grating elements. Wang proposed a single-layer zero elimination dual channel grating under normal incidence [20]. Xiang et al. proposed a five-port transmission grating with single-groove structure [21]. Fu et al. proposed a four-port grating with T-ridges arrays [22]; in addition, Huang et al. proposed a terahertz uniform beam splitter [23].

In this paper, a transmission four-port grating beam splitter with zero order suppression is proposed. In the case of normal incidence, rigorous coupled wave analysis (RCWA) [24-26] and simulated annealing algorithm (SAA) [27] were chosen to optimize the grating parameters with satisfactory results, and the optimized grating has high diffraction efficiency, good uniformity and polarization-independent properties. In addition, the finite element method (FEM) [28,29] was used to verify the results of RCWA calculations and to analyze the electric field distribution of the grating. The diffraction phenomena of the grating were also resolved by the simplified modal method (SMM) [30]. Considering practical applications, the incidence characteristics and processing tolerances of the grating were analyzed. The results show that the grating has good incidence angle bandwidth and processing tolerance.

2. The single-groove four-port grating with polarization independence

Fig. 1 shows a single-groove four-port transmission grating based on normal incidence. As shown in Fig. 1, the material of the grating ridge and the connecting layer is HfO_2 with a refractive index of n_2=1.8862 [31, 32], HfO_2 is an optical material with high refractive index, high transmittance, and low scattering loss, which is ideal for manufacturing high efficiency transmission gratings due to its low absorption and scattering loss of light waves. In addition, HfO_2 maintains a stable refractive index near 800 nm and has a wide wavelength tolerance bandwidth, which is of great importance for practical applications. The material of the grating substrate is fused silica with a refractive index of n_3=1.45, and the grating groove medium is air with a refractive index of n_1=1.00. In the single-groove, four-port transmission grating structure, d represents the grating period, h_1 denotes the thickness of

the grating ridge, *b* indicates the width of the grating ridge, h_2 is the thickness of the connecting layer, and the duty cycle of the grating is *f=b/d*. In the case of normal incidence, the incident beam with a wavelength of 800 nm is incident on the upper surface of the grating. After the incident light passes through the grating layer, the energy of the incident light is mainly diffracted to ±1st and ±2nd orders.

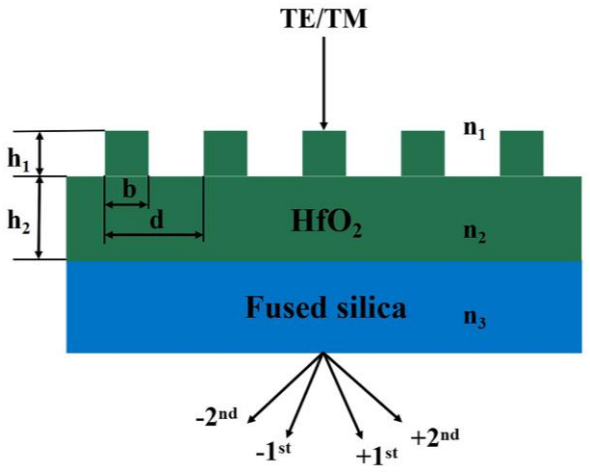

(a)

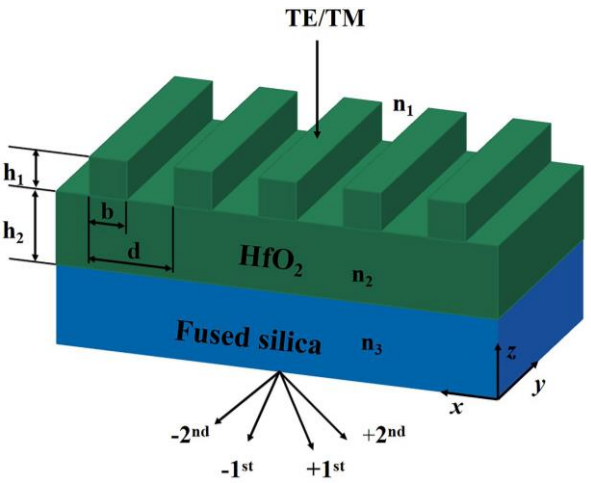

(b)

Fig. 1. Two-dimensional (a) and three-dimensional (b) diagrams of four-port grating with zero elimination transmission under normal incidence

In order to minimize the 0th order diffraction efficiency under TE and TM polarization and to improve the diffraction efficiency and diffraction uniformity of ±1st and ±2nd orders, we optimize the grating parameters (*d, h1, h2, f*) using RCWA combined with simulated annealing algorithm (SAA). RCWA is used to calculate the grating diffraction efficiency, and SAA is used to find the global optimal solution randomly in the solution space, the objective function of the SAA method is:

$$\varphi(d, h_1, h_2, f) = [1 - (E_{total} - |E_{-1} - E_{-2}|)], \quad (1)$$

where E_{total} represents the sum of diffraction efficiencies of non-zero diffraction orders under TE or TM polarization, E_{-1} and E_{-2} are the diffraction efficiencies of -1st and -2nd orders under TE or TM polarization, respectively, and the optimal parameters are obtained when the cost function reaches the minimum value. In order to realize the polarization insensitivity property, both TE polarization and TM polarization must be considered, so Eq. (1) should be further expressed as:

$$\varphi = \frac{\varphi_{TE} + \varphi_{TM}}{2}, \quad (2)$$

where φ_{TE} and φ_{TM} are the cost functions of TE polarization and TM polarization, respectively. Under the condition of incident wavelength λ=800 nm, the optimal parameters are obtained after calculation, as shown in Table 1.

Table 1. The Optimized parameters of single-groove four-port grating structure

λ	d	f	h_1	h_2
800 nm	1.455 μm	0.4	0.595 μm	1.398 μm

Under normal incident conditions, due to the symmetry of the periodic structure, the +1st order and - 1st order transmission efficiencies of TE and TM polarization are equal, and the +2nd order and -2nd order transmission efficiencies are also equal. So in the following calculation, we only consider the efficiency of 0th, - 1st, and -2nd orders. Fig. 2 shows the relationship between the transmission efficiency of the four-port grating beam splitter and the thickness of the grating ridge and the thickness of the connecting layer. It can be seen from Fig. 2 that at the depths of h_1=0.595 μm and h_2=1.398 μm, the efficiency of TE polarization at 0th, -1st, and -2nd orders are 0.73%, 24.24%, and 24.34%, respectively. Under TM polarization, the efficiency of 0th, -1st, and -2nd orders are 0.95%, 24.16%, and 23.21%, respectively. The transmission efficiency of 0th order under TE and TM polarization both close to 0. For the same grating structure, TE and TM polarizations can simultaneously output high efficiency and uniformity, which indicates that the beam splitter has polarization-independent characteristics.

Table 2. Comparison of efficiencies between this work and reported Refs. [22,23]

Scheme	$\eta_{\pm1}^{TE}$ (%)	$\eta_{\pm2}^{TE}$ (%)	$\eta_{\pm1}^{TM}$ (%)	$\eta_{\pm2}^{TM}$ (%)
Ref. [22]	22.17%	21.77%	24.12%	21.93%
Ref. [23]	23.06%	23.06%	/	/
This work	24.24%	24.34%	24.16%	23.21%

Table 2 shows the efficiency comparison between this

work and the reported references. It can be seen from Table 2 that compared with Ref. [23], the grating proposed in this paper not only improves the diffraction efficiency, but also has polarization-independent characteristics. Compared with Ref. [22], the grating proposed in this paper also has the advantage of higher efficiency.

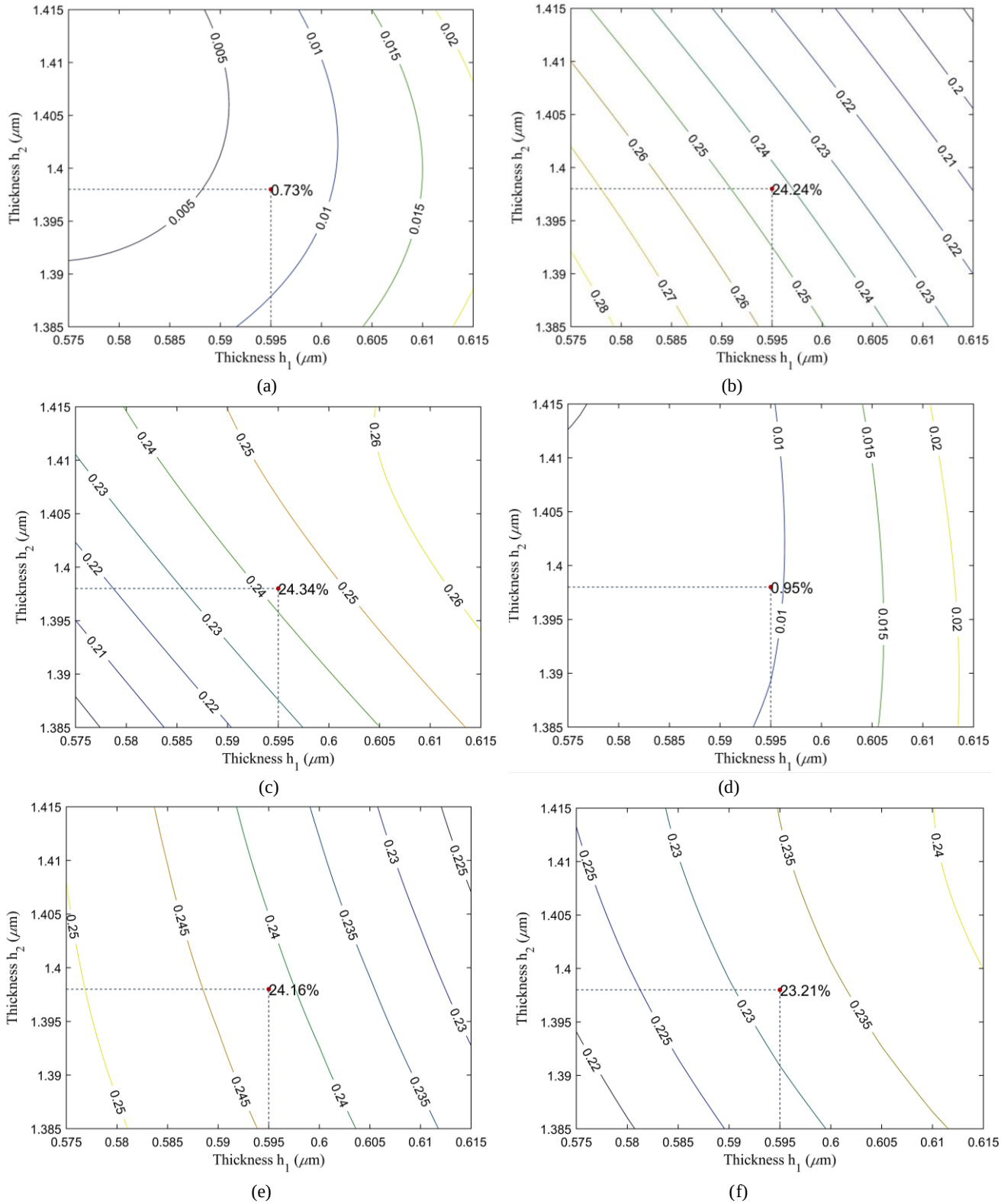

Fig. 2. Efficiencies in orders for the grating versus thicknesses of two layers under both two polarizations at wavelength of 800 nm under normal incidence: (a) efficiency of the 0th order for TE polarization, (b) efficiency of the -1st order for TE polarization, (c) efficiency of the -2nd order for TE polarization, (d) efficiency of the 0th order for TM polarization, (e) efficiency of the -1st order for TM polarization, (f) efficiency of the -2nd order for TM polarization, where d=1.455 μm and f=0.4 (color online)

Based on the optimized grating parameters in Table 1, the electric field distribution of the grating was calculated using the finite element method, and the results calculated using RCWA were verified. Fig. 3 shows the normalized electric field distribution of the four-port transmission grating under the effect of two polarizations. In addition, to explain the grating diffraction phenomena for the optimized grating parameters, the simplified modal method (SMM) is used in this paper. First, when the incident light is incident to the grating region, the beam-grating interaction can be described as:

$$\cos(\frac{2\pi d \sin\theta}{\lambda}) = F\left(n_{eff}^2\right), \tag{3}$$

where θ is the incident angle, n_{eff}^2 is the effective refractive index of the excited state discrete mode, and $F(n_{eff}^2)$ is the eigenfunction of the incident light in the grating region. Under normal incidence, $F(n_{eff}^2)$=1 is obtained by Equation (3). For TE polarization, $F(n_{eff}^2)$ can be expressed as:

$$F(n_{eff}^2) = \cos(\beta f d)\cos[\gamma(1-f)d] - \frac{\beta^2+\gamma^2}{2\beta\gamma}\sin(\beta f d)\sin[\gamma(1-f)d] \quad , \tag{4}$$

and for TE polarization, $F(n_{eff}^2)$ can be expressed as:

$$F(n_{eff}^2) = \cos(\beta f d)\cos[\gamma(1-f)d] - \frac{n_g^4\beta^2+n_r^4\gamma^2}{2n_g^4n_r^4\beta\gamma}\sin(\beta f d)\sin[\gamma(1-f)d] \quad , \tag{5}$$

where β and γ can be expressed as:

$$\beta = \frac{2\pi}{\lambda}\sqrt{n_r^2 - n_{eff}^2} \ , \ \gamma = \frac{2\pi}{\lambda}\sqrt{n_g^2 - n_{eff}^2} \ .$$

n_r and n_g denote the refractive indices of the grating ridge and grating groove, respectively. Fig. 4 shows the relationship curve between n_{eff}^2 an $F(n_{eff}^2)$ for λ=800 nm, duty cycle f=0.4, and d=1.455 μm. The dashed line $F(n_{eff}^2)$=1 indicates normal incidence, and it can be seen from the figure that the characteristic curves of TE and TM polarization have five intersections with the line, i.e., five propagation modes are excited in the grating layer. The effective refractive indices of the five modes in the grating are calculated by Eqs. (4,5), as shown in Table 3(a).

In Fig. 3, it can be seen that the energy distribution in the grating visualizes the complete superposition of all modes of incident light excitation within the grating. During the diffraction of the grating, two energy coupling processes take place. The first coupling process occurs when the incident light is incident into the grating region, and this process can be expressed by the integral equation [6] as:

for TE polarization:

$$\langle E_y^{in}(x) \leftrightarrow u_m(x)\rangle = \frac{\left|\int_0^d E_y^{in}(x)u_m(x)\,dx\right|^2}{\int_0^d|E_y^{in}(x)|^2\,dx\int_0^d|u_m(x)|^2\,dx} \ , \tag{6}$$

for TM polarization:

$$\langle H_y^{in}(x) \leftrightarrow u_q(x)\rangle = \frac{\left|\int_0^d H_y^{in}(x)u_q(x)\,dx\right|^2}{\int_0^d|H_y^{in}(x)|^2\,dx\int_0^d|u_q(x)|^2\,dx} \ , \tag{7}$$

where $E_y^{in}(x)$ represents the incident electric field, $H_y^{in}(x)$ represents the incident magnetic field, $u_m(x)$ and $u_q(x)$represent the grating modes of TE and TM polarization, respectively. The second coupling process occurs between the grating modes and the diffraction orders. This process can be expressed by the integral equation as:

for TE polarization:

$$\langle E_{yj}(x) \leftrightarrow u_m(x)\rangle = \frac{\left|\int_0^d E_{yj}(x)u_m(x)\,dx\right|^2}{\int_0^d|E_{yj}(x)|^2\,dx\int_0^d|u_m(x)|^2\,dx} \ , \tag{8}$$

for TM polarization:

$$\langle H_{yk}(x) \leftrightarrow u_q(x)\rangle = \frac{\left|\int_0^d H_{yk}(x)u_q(x)\,dx\right|^2}{\int_0^d|H_{yk}(x)|^2\,dx\int_0^d|u_q(x)|^2\,dx} \ , \tag{9}$$

where $E_{yj}(x)$ and $H_{yk}(x)$ represent the diffraction orders of TE and TM polarization, respectively. By calculating Eqs. (6-9), the energy exchange relations between grating modes and diffraction levels can be obtained as shown in Table 3(b). In summary, the first energy coupling occurs when the incident light enters the grating layer, and the energy is coupled to the five grating modes. Then the second energy coupling occurs between the grating modes and the diffraction orders, and the energy of the five grating modes is coupled to the individual diffraction orders. It allows a more intuitive understanding of the grating diffraction.

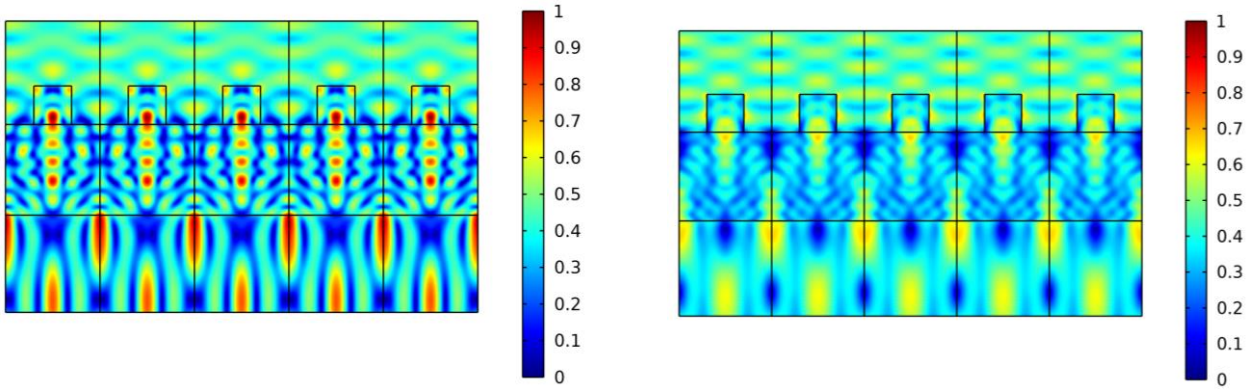

(a) (b)

Fig. 3. The normalized electric field distribution with λ=800 nm, d=1.455 μm, f=0.4, h_1=0.595 μm, h_2=1.398 μm: (a) TE polarization and (b) TM polarization (color online)

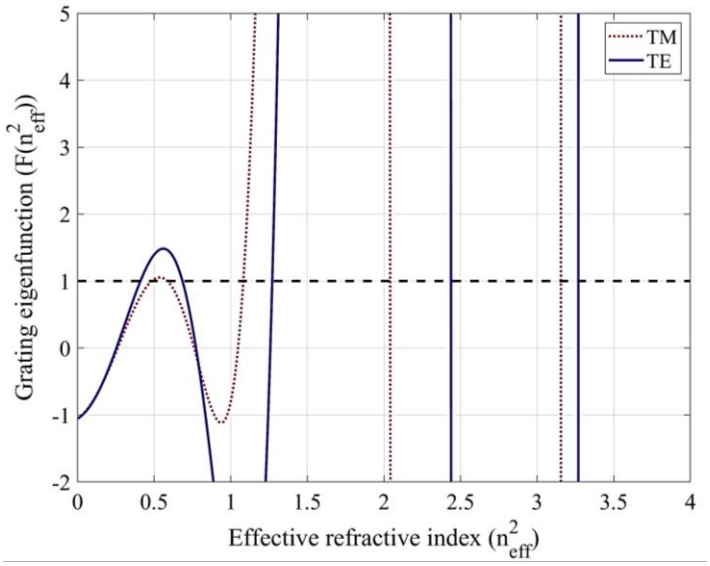

Fig. 4. Mode effective index of excitation in a grating medium with d=1.455 μm, f=0.4 (color online)

Table 3. Simplified modal method for the proposed four-port grating

(a) The effective refractive index n_{eff} of the grating layer

	n_{0eff}	n_{1eff}	n_{2eff}	n_{3eff}	n_{4eff}
TE	1.8080	1.5613	1.1274	0.8277	0.6410
TM	1.7763	1.4285	1.0402	0.7658	0.6955

(b) The coupling between the grating modes and diffraction orders

	Diffraction Order					
Mode	TE (0th)	TE (±1st)	TE (±2nd)	TM (0th)	TM (±1st)	TM (±2nd)
Mode 0	0.4633	0.2379	0.0297	0.3822	0.2419	0.0618
Mode 1	0	0.2728	0.1959	0	0.2015	0.2109
Mode 2	0.2932	0.0494	0.1994	0.4178	0.0838	0.1294
Mode 3	0.2277	0.2095	0.1281	0	0.1328	0.2177
Mode 4	0	0.2223	0.2290	0.0067	0.0894	0.2670

3. Analysis and discussions

In the process of optimizing the parameters, the incident wave is always incident normally. In practical applications, the incident angle and wavelength may affect the performance of the grating. It is necessary to consider the bandwidth of incident wavelength and incident angle. Fig. 5 shows the relationship between the diffraction efficiency of the grating and the incident wavelength. When the incident wavelength is in the range of 793-807 nm, the efficiencies of the -1st and -2nd orders are both higher than 20% for TE polarization and the bandwidth is 10 nm. when the incident wavelength is in the range of 780-813 nm, the efficiencies of the -1st and -2nd orders are both higher than 20% for TM polarization, and the bandwidth is 33 nm. The results show that the grating has good bandwidth under TM polarization.

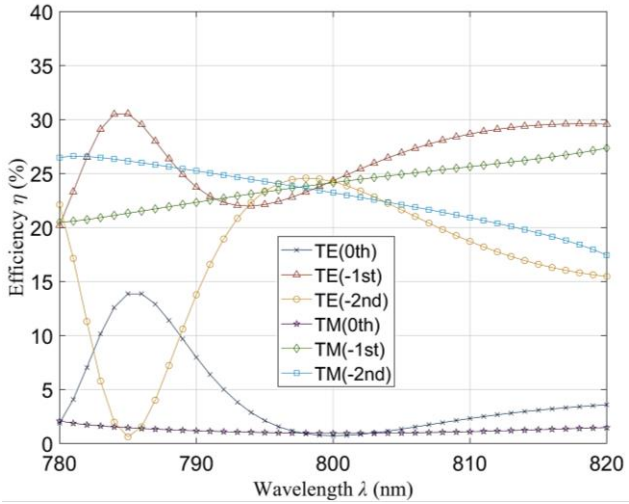

Fig. 5. The efficiency corresponding to the incident wavelength: TE polarization and TM polarization, where d=1.455 μm, f=0.4, h_1=0.595 μm and h_2=1.398 μm (color online)

Fig. 6 shows the effect of the angle of incidence on the diffraction efficiency of the grating. For TE polarization, the efficiencies of the ±1st and ±2nd orders are both higher than 20% at an incidence angle of -1.3° to 1.3°. For TM polarization, the efficiency of ±1st and ±2nd orders is higher than 20% when the incident angle is -2.2° to 2.2°. The grating has a good bandwidth of incident angle. The deviation of the incident angle from the zero angle affects the performance to some extent, and a good incident angle bandwidth is of practical application.

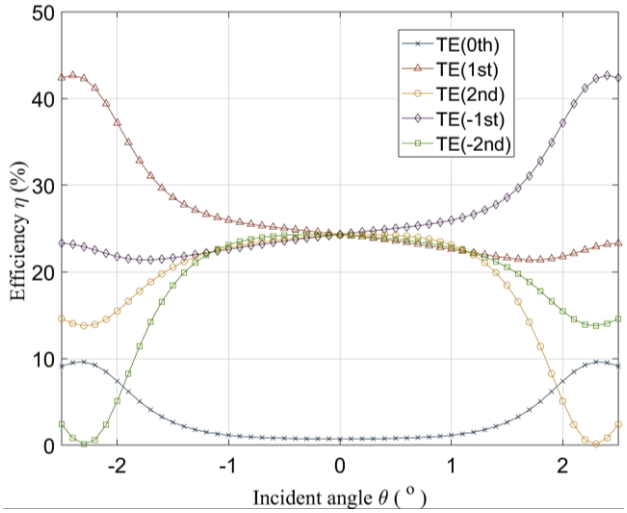

(a)

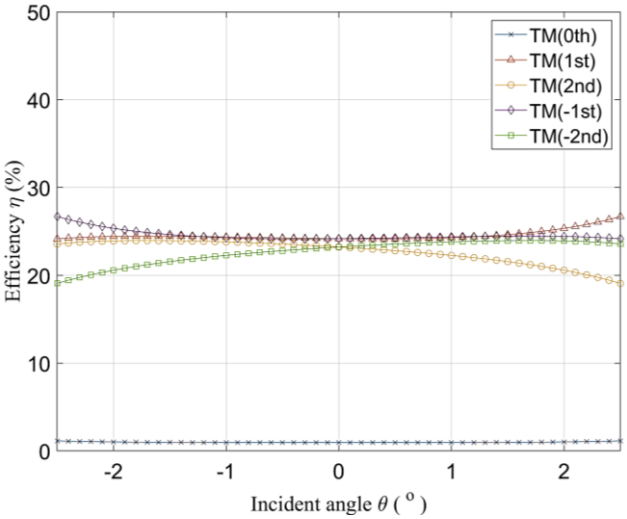

(b)

Fig. 6. The diffraction efficiency corresponding to the incident angle for the incident wavelength of 800 nm with the optimized grating profile parameters: (a) TE polarization and (b) TM polarization, where d=1.455 μm, f = 0.4, h_1=0.595 μm and h_2=1.398 μm (color online)

Due to the control accuracy and micromachining technology, there are manufacturing tolerances for the period and duty cycle of the grating. Therefore, it is vital to analyze the process tolerance of each structural parameter of the grating for the actual preparation of the grating. Fig. 7 shows the relationship between the diffraction efficiency of the grating and the grating period at two polarizations. The horizontal axis is the grating period, and the vertical axis is the grating efficiency. When the grating period is between 1428-1471nm, the non-zero orders diffraction efficiency for TE and TM polarization is still higher than 20%. Fig. 8 shows the relationship between diffraction efficiency and duty cycle. It is clear

from Fig. 8 that the -1st and -2nd orders diffraction efficiencies of TE and TM polarizations are the best when the duty cycle is 0.4. When the duty cycle is between 0.38 and 0.46, the diffraction efficiency of the -1st and -2nd orders for TE and TM polarization is still higher than 20%. The above analysis results show that the grating structure has good process tolerance in terms of both period and duty cycle, which is of great importance for practical production.

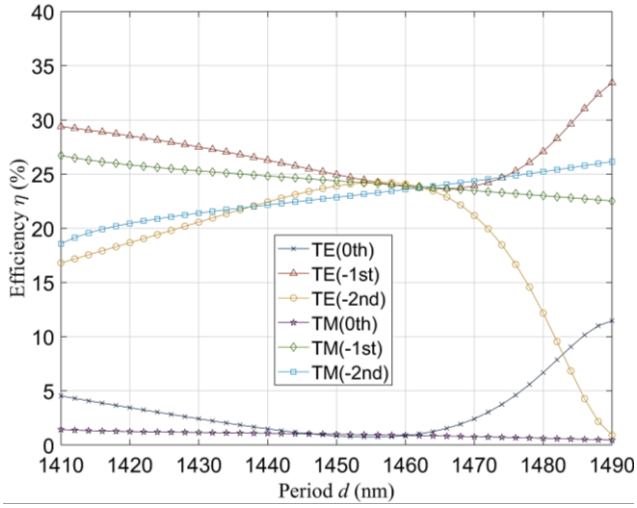

Fig. 7. The efficiency corresponding to the period under normal incidence: TE polarization and TM polarization, where f= 0.4, h_1= 0.595 μm and h_2= 1.398 μm (color online)

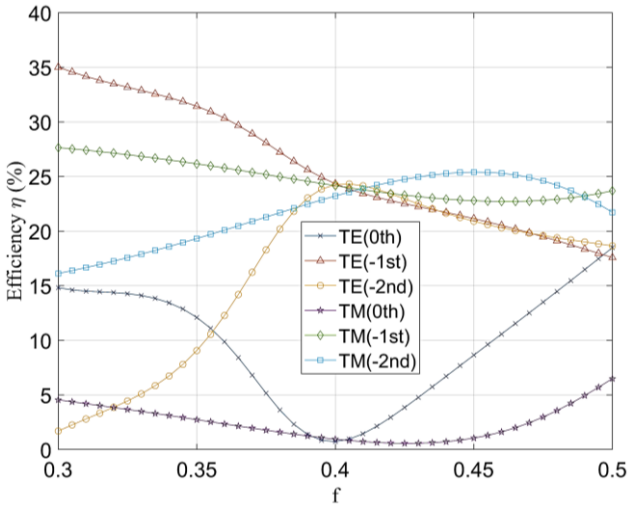

Fig. 8. The efficiency corresponding to duty cycle under normal incidence: TE polarization and TM polarization, where d=1.455 μm, h_1=0.595 μm and h_2=1.398 μm (color online)

4. Conclusion

In this paper, a transmission four-port grating beam splitter with 0th order rejection is proposed. The structural parameters of the grating are optimized with RCWA and SAA, and the grating has high diffraction efficiency and polarization-independent characteristics under the optimal structural parameters. For TE polarization, the efficiencies of ±1st and ±2nd orders are 24.24% and 24.34%, respectively, for TM polarization, the efficiencies of ±1st and ±2nd orders are 24.16% and 23.21%, respectively. Meanwhile, the 0th order diffraction efficiency at both polarizations is close to 0. In addition, FEM and SMM are used to describe the electric field distribution and diffraction phenomena of the grating, and then to explain the energy coupling process in the grating. Finally, the incidence characteristics and process tolerances are investigated by RCWA method. The results show that the grating has good bandwidth and process tolerance.

Acknowledgements

This work is supported by the Science and Technology Program of Guangzhou (202002030284, 202007010001).

References

[1] S. Wang, Z. Zhang, F. Meng, P. Wang, Optoelectron. Adv. Mat. **15**(11-12), 515 (2021).
[2] Z. R. Ghayib, A. A. Hemed, Optoelectron. Adv. Mat. **16**(7-8), 307 (2022).
[3] Z. L. Hussain, R. S. Fyath, Optik **251**, 168449 (2022).
[4] H. Jiang, D. Li, X. Zhang, Z. Ma, T. Lu, X. Shao, Optik **247**, 167997 (2021)
[5] D. Wu, T. Zheng, L. Wang, X. Chen, L. Yang, Z. Li, G. Wu, Opt. Laser Technol. **145**, 107477 (2022).
[6] H. Li, T. Huang, L. Lu, Z. Hu, B. Yu, Opt. Laser Technol. **145**, 107465 (2022).
[7] Z. Huang, B. Wang, Opt. Mater. **125**, 112065 (2022).
[8] J. Cheng, B. Fan, W. Chen, Z. Su, Optoelectron. Adv. Mat. **16**(7-8), 277 (2022).
[9] W. He, Y. Liu, Z. Luo, X. Chen, G. Hu, C. Zhu, L. Zhu, Optoelectron. Adv. Mat. **16**(9-10), 391 (2022).
[10] R. Xiao, L. Wang, J. Wang, H. Yan, H. Cheng, Optik **259**, 169041 (2022).
[11] W. Li, S. Chen, Y. Chu, P. Huang, G. Yan, Optik **262**, 169290 (2022).
[12] Z. Huang, B. Wang, Surf. Interfaces **31**, 101987 (2022).
[13] N. Jellali, M. Ferchichi, M. Najjar, Optik **244**, 166188 (2021).
[14] Z. L. Hussain, R. S. Fyath, Optik **264**, 169456 (2022).
[15] P. Tian, W. Bi, X. Wang, W. Jin, B. Zhang, X. Fu, G. Fu, Optik **231**, 166461 (2021).
[16] B. Wu, B. Zhang, W. Liu, Q. Lu, L. Wang, F. Chen, Opt. Laser Technol. **145**, 107500 (2022).
[17] Y. Xie, W. Jia, C. Xiang, P. Sun, C. Wei, C. Zhou, Opt Commun. **483**, 126669 (2021).
[18] F. Chen, J. Zhang, J. Ma, C. Wei, R. Zhu, B. Han, Q. Wang, Opt. Commun. **444**, 45 (2019).

[19] X. Tian, Y. Wang, Q. Zhao, Y. Li, H. Li, J. Qu, D. Zhang, Optik **248**, 168054 (2021).
[20] B. Wang, Sci. Rep. **5**, 16501 (2015).
[21] C. Xiang, C. Zhou, W. Jia, J. Wu, Chin. Opt. Let. **16**(7), 070501 (2018).
[22] C. Fu, B. Wang, Laser Phys. **30**, 116203 (2020).
[23] H. Huang, S. Ruan, T. Yang, P. Xu, Nano-Micro Lett. **7**, 177 (2015).
[24] M. G. Moharam, D. A. Pommet, E. B. Grann, T. K. Gaylord, J. Opt. Soc. Am. A **12**(5), 1077 (1995).
[25] X. Zhu, B. Wang, Z. Xiong, Y. Huang, Optik **260**, 169049 (2022).
[26] Z. Xu, T. Lyu, X. Sun, Opt. Commun. **451**, 17 (2019).
[27] V. Cerny, J. Optim. Theory Appl. **45**, 41 (1985).
[28] J. Lin, X. Shen, R. Li, Opt. Express **28**(15), 22978 (2020).
[29] E. Elashamla, S. Hekal, L. Gomaa, Opt. Commun. **457**, 124621 (2020).
[30] I. C. Botten, M. S. Craig, R. C. Mcphedran, J. L. Adams, J. R. Andrewartha, Opt. Acta **28**(3), 413 (1981).
[31] M. F. Al-Kuhaili, Optical Materials **27**, 383 (2004).
[32] A. Kompa, D. Kekuda, M. S. Murari, K. M. Rao, Optical Materials **136**, 113424 (2023).

*Corresponding author: wangb_wsx@yeah.net